

Investigation of Bragg surface diffraction in semiconductors and epitaxial structures by reciprocal-space analysis

S. L. MORELHÃO^{a*} AND E. ABRAMOF^b

^aDepartamento de Física Aplicada, USP, CP 66318, 05315-970 São Paulo, SP, Brazil, and ^bInstituto Nacional de Pesquisas Espaciais, LAS, CP515, 12201-970 São José dos Campos, SP, Brazil. E-mail: morelhao@if.usp.br

(Received 31 March 1999; accepted 19 May 1999)

Abstract

Bragg surface diffraction (BSD) is a special case of three-beam diffraction, where the secondary beam is scattered in the surface-parallel direction. Under the BSD condition, the surface-detour reflection (secondary plus coupling reflections) transfers some of the secondary-beam intensity into the monitored primary beam. The extinction regime in which such transfer takes place depends on the crystalline perfection of the surface. Based on this fact, the mapping of the BSD profile, in an ω : φ scan technique, has been proposed [Morelhão & Cardoso (1996). *J. Appl. Cryst.* **29**, 446–456] as a method to obtain information on the in-plane crystalline quality of the surface. With the X-ray optics for BSD mapping, the diffracting surface thickness that defines the profile could not be measured or compared with those under conventional Bragg diffraction. In this report, the BSD using a triple-axis diffractometer is investigated. Reciprocal-space mapping of the Bragg reflection (primary reflection) was performed *in* and *out* of the BSD condition. It reveals the diffracting surface thickness of BSD in GaAs and Si substrates. The triple axis was also used to investigate the BSD in the SiGe multiple quantum well, and it has demonstrated the existence of effective satellite peaks for such structures.

1. Introduction

High-resolution X-ray diffraction techniques, such as double-crystal rocking-curve and reciprocal-space mapping, or rod scans, are powerful techniques for analysing semiconductor epitaxial structures. They provide information on periodicity of superlattices and multiple quantum wells, lattice mismatch (relaxation of the structure), and crystalline perfection of the layer. These techniques investigate the X-ray scattering by the structures under two-beam diffraction conditions (one Bragg reflection). Under these conditions, all features relevant to the diffraction physics are described in the incidence plane, *i.e.* the plane defined by the incident and diffracted beams. The diffraction geometry is two-dimensional. Consequently, in the commercially available ready-to-use diffractometers for high-resolution

diffraction, the X-ray optics restrict the beam divergence only in the incidence plane.

A natural step forward in the development of other X-ray analytical tools has been the investigation of the three-beam diffraction phenomenon (Chang, 1984; Weckert & Hümmel, 1997). This phenomenon arises when an incident monochromatic beam simultaneously satisfies the Bragg law for two sets of lattice planes within a crystal. The three-beam diffraction is systematically generated when the crystal is first aligned by an ω rotation for a symmetric Bragg reflection, the primary reflection 01. The φ rotation of the crystal around the reciprocal lattice vector of the primary reflection, \mathbf{H}_{01} , causes another reflection, secondary reflection 02, to diffract the incident beam (\mathbf{k}_0 , wavevector) simultaneously. Bragg surface diffraction (BSD) is a special case of three-beam diffraction, where the secondary beam ($\mathbf{k}_2 = \mathbf{H}_{02} + \mathbf{k}_0$) is scattered in the surface-parallel direction. Under the BSD condition, the secondary beam is diffracted towards the primary beam (\mathbf{k}_1) direction by the coupling reflection 21. It is mathematically expressed by $\mathbf{k}_1 = \mathbf{H}_{21} + \mathbf{k}_2 = \mathbf{H}_{01}^* + \mathbf{k}_0$, where $\mathbf{H}_{01}^* = \mathbf{H}_{21} + \mathbf{H}_{02}$ is the reciprocal vector of the effective primary reflection. The 01* reflection, also known as the surface-detour reflection, usually modifies the monitored primary intensity. Its geometrical condition, *i.e.* the incident-beam direction $\mathbf{k}_0 = \mathbf{k}_0(\omega, \varphi)$, can be calculated by solving the equations

$$\mathbf{k}_0 \cdot \mathbf{H}_{02} = -|\mathbf{H}_{02}|^2/2 \quad (1)$$

and

$$\mathbf{k}_0 \cdot \mathbf{H}_{21} = -|\mathbf{H}_{21}|^2/2 - \mathbf{H}_{02} \cdot \mathbf{H}_{21},$$

which are derived from the Bragg diffraction condition for secondary and coupling reflections, respectively, and by replacing $\mathbf{k}_2 = \mathbf{H}_{02} + \mathbf{k}_0$ in the second equation. The reciprocal-space Ewald construction of the BSD is shown in Fig. 1(a), together with a scheme of the surface-detour reflection (Fig. 1b).

The BSD geometry is three-dimensional since the incident beam has to fulfill one specific (ω, φ) direction to excite the surface-detour reflection. Therefore, the BSD presents two profiles, one for the ω scan and another for the φ scan. Thus, the X-ray optics for the

incident beam have to be concerned with the directions parallel and perpendicular to the primary incidence plane. With a circularly collimated incident beam, the BSD mapping can be carried out by combining ω and φ scans ($\omega:\varphi$ scan). This technique has shown that the profile of the BSD has good sensitivity to the crystalline perfection of the surface; it is affected by surface finishing processes of semiconductor substrates, lattice

reduction in porous silicon and surface damage due to ion implantation (Morelhão & Cardoso, 1996; Hayashi *et al.*, 1997). However, the X-ray optics for properly mapping the BSD present a strong limitation for the wide use of the technique. With commercially available diffractometers, this technique cannot be performed without significant instrumental modifications. On the other hand, the penetration-depth value of the surface-detour reflection can not be measured by the $\omega:\varphi$ scan technique; it investigates only the incident-beam direction. Such a value has not even been estimated theoretically. The three-beam dynamical theory (Weckert & Hümmer, 1997) has not been able to handle the BSD due to the unusual boundary condition for the secondary beam. Its propagation direction is parallel to the surface.

In this work, we analyse the reciprocal space of the effective primary reflection, or the surface-detour reflection, for a triple-axis diffractometer. Reciprocal-space mapping and rod scans were performed *in* and *out* of the BSD condition for GaAs and Si substrates as well as for SiGe/Si superlattices. The results and their importance are discussed below.

2. Experimental

The measurements were carried out using a Philips X'Pert (MRD) diffractometer using the triple-axis configuration. It employs a four-crystal Ge(220) monochromator in the incident-beam optics, which gives a horizontal divergence of 12 arcsec for Cu $K\alpha_1$ radiation. A channel-cut Ge(220) analyser crystal selects the direction of the primary beam (the beam diffracted by the primary reflection 01), also with a resolution of 12 arcsec. Recently, a number of authors have described in detail the power of this technique for the characterization of heterostructures (Fewster, 1991; Bauer & Koppensteiner, 1995).

The 002/111 BSD was chosen for our investigation. The primary reflection of this BSD is the 002 Bragg symmetric reflection (\mathbf{H}_{01}), and the 111 secondary reflection (\mathbf{H}_{02}) plus the $\bar{1}\bar{1}1$ coupling reflection (\mathbf{H}_{21}) give the 002* surface-detour reflection. A weak or forbidden primary reflection is necessary in order to enhance the contribution of the surface-detour reflection. The $[1\bar{1}0]$ direction was taken as the reference direction, $\varphi = 0$.

3. Results and discussion

3.1. Attenuation of Bragg surface diffraction in GaAs and Si

Reciprocal-space maps around the 002 reflection alone ($\varphi = 0$) and under BSD ($\varphi \simeq 6^\circ$) for a GaAs wafer

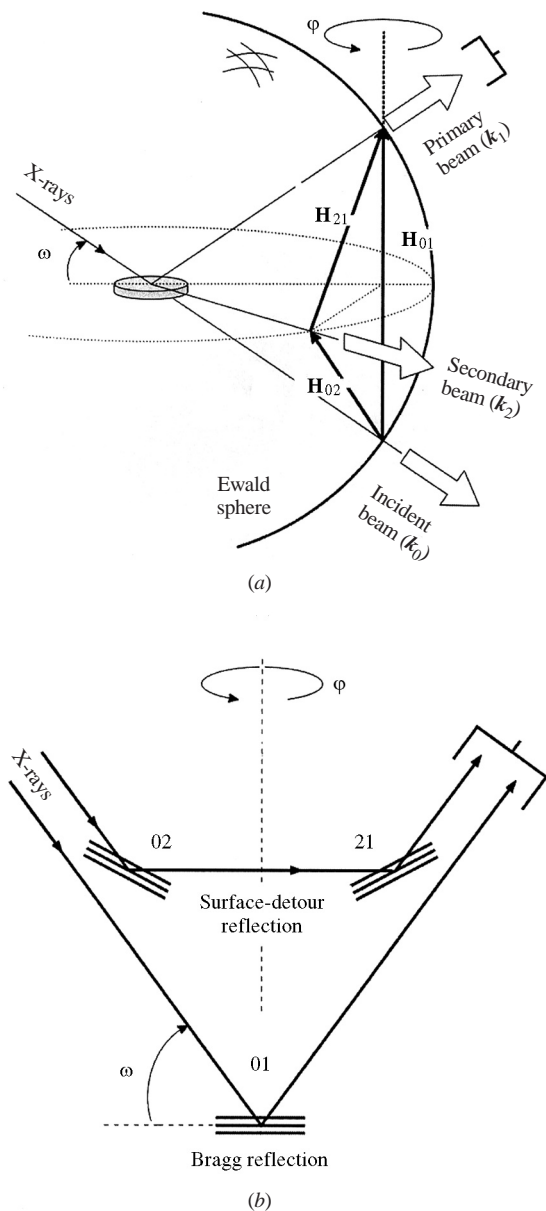


Fig. 1. Bragg surface diffraction (BSD) geometry. (a) Three-dimensional Ewald construction for the primary (\mathbf{H}_{01}), secondary (\mathbf{H}_{02}) and coupling (\mathbf{H}_{21}) diffraction vectors. (b) Planar scheme to illustrate the surface-detour reflection: the 02 (surface secondary) reflection plus the 21 (coupling) reflection.

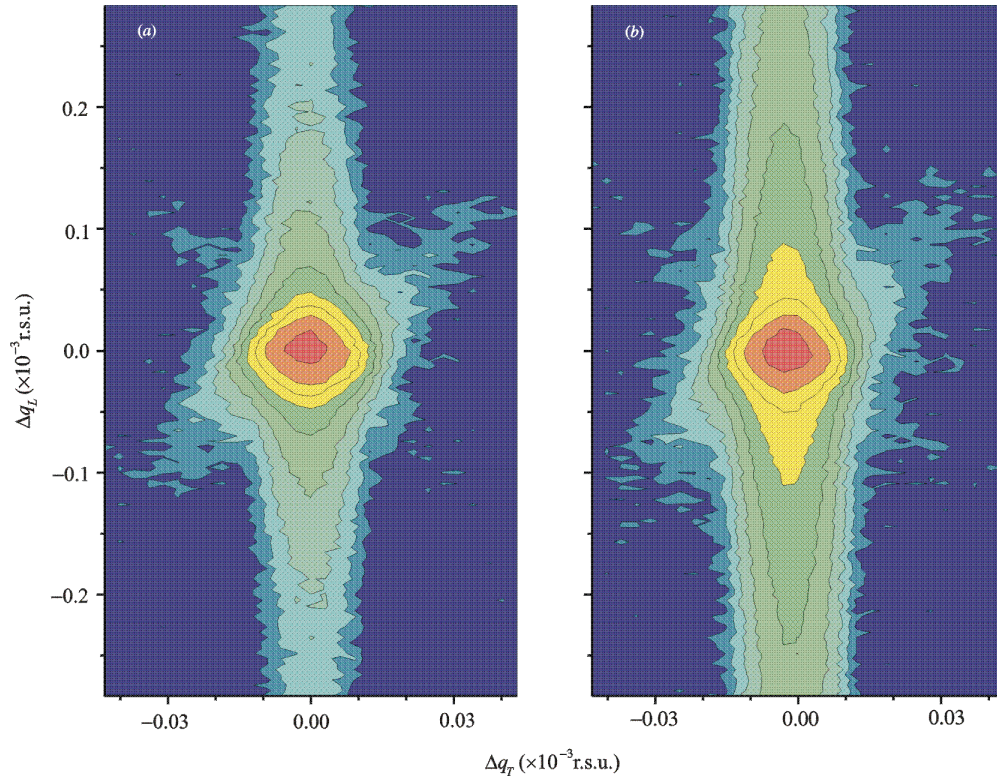


Fig. 2. Reciprocal-space mapping of the 002 Bragg symmetrical reflection: (a) out and (b) in the BSD condition. The Δq_L and Δq_T are the reciprocal-space distances (\AA^{-1}) from the centre of the rod in the longitudinal and transversal directions, respectively.

are shown in Fig. 2. The results confirm that the remarkable difference between them, which is the broadening of the peak when the 002* reflection is excited (Fig. 2b), is due to the elongation of the rod (the reciprocal-lattice points in real crystals are like rods) and not due to some mosaicity in the diffracting volume under BSD.

The attenuation of the X-ray wave field (amplitude) can be described by the function $s(z) = \exp(-\alpha z)$. It is estimated *via* a kinematical approach from the rod profile, $P(\Delta q)$, since the Fourier transformer relates them: $P(\Delta q) = |\int s(z) \exp(-2\pi i \Delta q z) dz|^2$. Hereinafter, $\Delta q = \Delta q_L$ (Fig. 2), the reciprocal-space distance from the centre of the rod in the longitudinal direction (along the rod).

The experimental intensities just along the rods, obtained from Fig. 2, are shown in Fig. 3 (squares). The simulated profiles (solid lines) are also shown. The profiles (tails) of the 002 rod, out of BSD, and of the 002* surface-detour rod (dashed line) were obtained with $\alpha = 0.35 \mu\text{m}^{-1}$ and $\alpha = 2.5 \mu\text{m}^{-1}$, respectively. The 002* rod was calculated in order to fit the experimental profile under BSD (open squares), when added to the experimental 002 profile (solid squares).

The intensity of the 002 reflection is much weaker than that of the $111 + \bar{1}\bar{1}\bar{1} = 002^*$ surface-detour (effective) reflection. However, the BSD appears weak

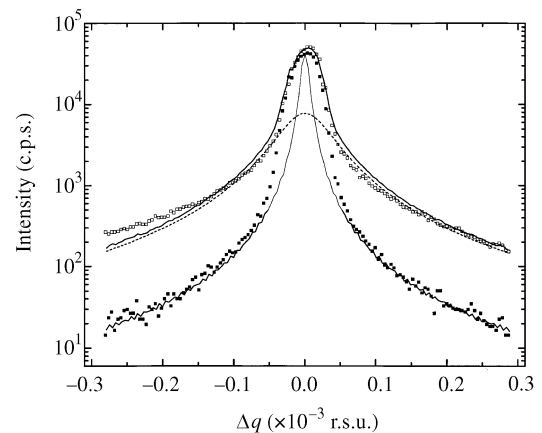


Fig. 3. Intensity profiles just along the rods from Figs. 2(a) (solid squares) and 2(b) (open squares). Simulated profiles are also shown (solid lines). The elongation of the surface-detour rod (dashed line) was calculated in order to fit the tails of the profile obtained by subtracting the first experimental profile from the second one.

here because the vertical divergence of the incident beam is not limited. It is about 1° and it all contributes to the 002 reflection, while only 3% ($\Delta\varphi \simeq 100$ arcsec) of the incident beam fulfills the BSD condition (Morelhão & Cardoso, 1996; Hayashi *et al.*, 1997).

The visible discrepancy between the experimental and simulated 002 profiles (at $\varphi = 0$) arises due to extinction effects. When the wave field propagates for a significant thickness of the crystal, the primary extinction reduces the intensities around the maximum of the rods. Therefore, if no extinction were present, the attenuation value for the 002 rod should be smaller than $0.35 \mu\text{m}^{-1}$. Although, the surface-detour rod is basically an extinction phenomenon along the surface-parallel direction, which transfers energy from the surface secondary beam to the primary one, less extinction effects should be evident in the rod profile, because the primary extinction along the surface-normal direction does not exist for the effective reflection. It is also interesting to note that the surface secondary beam is generated below the surface and is already inside the crystal; thus it is a quite different phenomenon from specular reflection and grazing incidence diffraction. The effects due to the in-plane extinction regime are clearly visible in the $\omega:\varphi$ scan of the BSD (Hayashi *et al.*, 1997).

By analysing BSD in crystals in which the Bragg reflection is forbidden, such as in silicon and germanium crystals, the reduction of the extinction effects on the surface-detour rod can be checked. In these crystals the observed 002/111 BSD intensities are defined only by the surface-detour reflection since the 002 reflection is completely forbidden. Fig. 4 shows the experimental (solid squares) and simulated (solid line) rod scan under the BSD condition for an Si(001) crystal. The simulated profile was calculated with $\alpha = 1.15 \mu\text{m}^{-1}$, and it matches the experimental one very well. This result implies that the surface-detour reflection can be seen as an effective

reflection of two-beam diffraction, free of primary extinction.

The attenuation of the wave field in the effective reflection for GaAs ($\alpha = 2.5 \mu\text{m}^{-1}$) is stronger than in Si ($\alpha = 1.15 \mu\text{m}^{-1}$) because the linear absorption coefficient as well as the reflectivity of the 111 planes are stronger in GaAs crystals. These attenuation lengths imply that the diffracting thicknesses of $0.3 \mu\text{m}$ (GaAs) and $0.7 \mu\text{m}$ (Si) provide 80% of the intensity diffracted by the effective reflections. In other words, these thicknesses are about the penetration depth of the BSD in GaAs and Si crystals.

In triple-axis diffractometers, the measurability of BSD from thin epitaxial layers and superlattices is limited by the intensity of the Bragg reflection. For instance, in GaAs buffer layers the rod scan of the surface-detour reflection could be obtained with better resolution than presented here if the vertical divergence is limited to about one minute of arc. When GaAlAs layers or superlattices are grown on top of the buffer layer, the reflectivity of Bragg reflection for these structures is stronger than for the GaAs, and then the resolution of the BSD is even worse. However, the BSD can be clearly observed in structures with forbidden primary reflection, as in $\text{Si}_x\text{Ge}_{1-x}/\text{Si}$ heterostructures.

3.2. Effective satellites in SiGe superlattices

In our investigation of BSD in SiGe superlattices by triple-axis diffractometry, one new feature of diffraction by superlattices has been observed, namely the occurrence of effective satellites. These are three-beam diffractions where the secondary and coupling reflections are the satellite reflections of the superlattice. For a better discussion of the results, a short introduction on two-beam diffraction of a superlattice is given in the next paragraph.

In general, by probing the reciprocal space of superlattices, several satellite rods are seen. If the period of a superlattice is $P = n_a d_a + n_b d_b$, the position of satellite rods with respect to the reciprocal-space origin is $q_s = s/P$, where $n_{a,b}$ are the numbers of monolayers (MLs), $d_{a,b}$ are the intermonolayer distances for a and b types of atoms (Ge and Si, in our case), and s is a positive integer. In the characterization of superlattices, the satellite at $q_s = (n_a + n_b)/P = 1/\langle d \rangle$ with $s = n_a + n_b$ has been labelled as the zeroth-order satellite (SL0). Then, the average lattice parameter of the superlattice, $\langle d \rangle$, defines the SL0 rod position and the positions of the other satellite rods are defined by P . Regarding the substrate reciprocal vectors, \mathbf{H}_{ij} , the structures of satellites can be expressed by vectors such as $\mathbf{H}_{ij}^{(n)} = \mathbf{H}_{ij} + (\Delta q_{ij} + n/P)\hat{z}$. The superscript n stands for the $0, \pm 1, \dots$ satellites at around the position of SL0 [$n = s - (n_a + n_b)$], \hat{z} is the surface-perpendicular direction and Δq_{ij} is the SL0 shift from

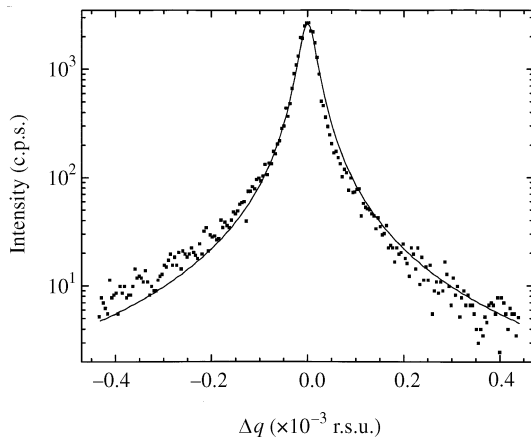


Fig. 4. Rod scan of the 002 Si reflection under BSD ($\varphi \simeq 6^\circ$): experimental (squares) and simulated (line).

Table 1. Measured values from 004 rod scans of a series of SiGe multiple shallow quantum wells

All samples have ten repeats of the period $P = n_a d_a + n_b d_b$ ($a = \text{Ge}$, $b = \text{Si}$). The values of $\Delta q/q^*$ ($\times 10^{-3}$) are from the 002* rod scans (Fig. 6).

Sample	Nominal		Experimental				
	n_{Ge}	n_{Si}	P ($\pm 0.24 \text{ \AA}$)	$\langle d \rangle$ ($\pm 0.000011 \text{ \AA}$)	$n_{\text{Ge}} + n_{\text{Si}}$ (± 0.2)	$\Delta q/q$ ($\pm 0.0082 \times 10^{-3}$)	$\Delta q/q^*$ ($\pm 0.016 \times 10^{-3}$)
SQW3	3	222	292.36	1.358901	215.2	-0.8656	-0.843
SQW4	4	222	294.27	1.359265	216.5	-1.1334	-1.020
SQW5	5	222	296.48	1.359675	218.1	-1.4344	-1.455
SQW6	6	222	286.20	1.360175	210.4	-1.8013	-1.827

the respective substrate reciprocal vector. The value of Δq_{ij} also depends on the z component of \mathbf{H}_{ij} , or on the L Miller index of the HKL substrate rod. For a given HKL reflection, $\Delta q_{HKL} = L/4\langle d \rangle - L/a_0 = L/a_0(a_0/4\langle d \rangle - 1)$. Then, $\Delta q/q$ ($= a_0/4\langle d \rangle - 1$) is constant since $q = \hat{z} \cdot \mathbf{H} = L/a_0$. It implies, for instance, that $\Delta q_{(HK4)} = 2\Delta q_{(HK2)} = 4\Delta q_{(HK1)}$.

The three-beam diffraction from satellite reflections generates effective satellites that are described by $\mathbf{H}_{01}^{(n+m)*} = \mathbf{H}_{02}^{(n)} + \mathbf{H}_{21}^{(m)}$, where n and m stand for the normal satellites at the 02 (secondary) and 21 (coupling) reflections, respectively. Since $\Delta q_{02} = \Delta q_{21} = \Delta q_{01}/2$ (BSD geometry), $\mathbf{H}_{01}^{(n+m)*} = \mathbf{H}_{02} + \mathbf{H}_{21} + [\Delta q_{02} + \Delta q_{21} + (n+m)/P]\hat{z} = \mathbf{H}_{01}^* + [\Delta q_{01} + (n+m)P]\hat{z}$. Therefore, they are lined up along the z direction and their diffraction condition can be fulfilled in the rod scan of the 01 reflection. The effective satellite of order p ($\text{SL}p^*$) has contributions from all detour reflections where $n+m=p$ and its position is the same as the normal $\text{SL}p$ satellite around the 01 reflection. For instance, the zeroth-order effective satellite, $\text{SL}0^*$, has contributions from all detour reflections where $n+m=0$. However, only in detour reflections with $n=m$, is the secondary beam in the surface-parallel direction, as in BSD.

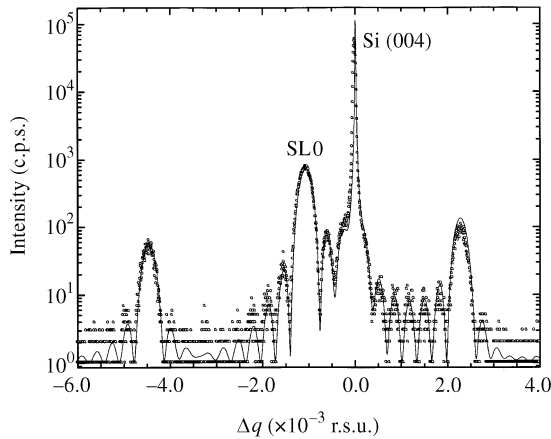


Fig. 5. Rod scan of the 004 reflection ($\varphi = 0$) for sample SQW5 (Table 1): experimental (circles) and calculated spectrum (solid line). The zeroth-order satellite peak ($\text{SL}0$) is at $\Delta q = -1.0567$ (60) $\times 10^{-3} \text{ \AA}^{-1}$.

The φ angles for exciting the $\text{SL}p^*$ satellites are obtained by solving equation (1) for $\mathbf{H}_{02}^{(n)}$ and $\mathbf{H}_{21}^{(m)}$. The angle, α , of the secondary-beam direction with the surface plane depends on the n and m indices according to $\sin \alpha = \lambda \mathbf{H}_{02} \cdot \hat{z} + \lambda [\Delta q_{02} + n/P] - \lambda |\mathbf{H}_{01}^{(n+m)*}|/2$. Note that the φ and α angles are different for each set of n and m , even with the constrain $n+m=p$.

The occurrence of effective satellites was investigated in a series of four SiGe multiple shallow quantum wells, described in Table 1. Fig. 5 shows the rod scan ($\omega/2\theta$ scan) of the 004 reflection for sample SQW5. The full line is the calculated spectrum, using the Takagi-Taupin equation (Bartels *et al.*, 1986), which best fitted the measured data. In this calculation, the quantum-well structure is assumed to be coherent, *i.e.* the in-plane lattice constant is the same as that of the Si substrate throughout the whole structure. Three satellite peaks (-1 , 0 and $+1$) are visible in the presented scan interval, and the $\text{SL}0$ satellite peak is shifted from the 004 Si substrate peak by $\Delta q/q = -1.4344$ (82) $\times 10^{-3}$. The other samples were also characterized: the 004 rod scans were very similar to that in Fig. 5; the measured values are presented in Table 1.

The rod scans of the 002 reflection under normal diffraction conditions (two beam, $\varphi = 0$) did not presented any diffracted intensity since it is a forbidden reflection for both the Si and the Ge lattice. The effective satellites, as well as the substrate BSD, are observed by performing a rod scan at a φ position near the BSD condition ($\varphi \simeq 6^\circ$): 002* rod scans. The scans for the samples are shown in Fig. 6. The measured shift, $\Delta q/q^*$, of each $\text{SL}0^*$ satellite peak from the substrate BSD peak is also listed in Table 1; they are the same as the values obtained from the 004 rod scans. For sample SQW5, very low counts were measured at the positions of the $\text{SL}-1^*$ and $\text{SL}+1^*$ satellites (insets of Fig. 6).

The calculated values of Δq and $\Delta\varphi$, regarding the position of the 002* Si rod, as well as the α angles are shown in Table 2 for the $\text{SL}p^*$ satellites of sample SQW5. The vertical divergence of the incident beam fulfills the azimuthal condition for several effective satellites. However, in most cases their intensities are not strong enough to be measured. Only the $\text{SL}0^*$ peaks are clearly observed in these samples. The fact that the secondary beam is not in the surface-parallel direction

Table 2. Calculated Δq and $\Delta\varphi$ shifts (regarding the 002^* substrate rod) of the effective satellites for sample SQW5 ($\Delta q/q = -14344 \times 10^{-3}$) along with the calculated α angles for these satellites

n	m	SL p^*	$\Delta q (\times 10^{-3} \text{ \AA}^{-1})$	$\Delta\varphi$ (arcsec)	α (arcsec)
0	0	0	-0.54	-60	0
+1	-1	0	-0.54	-70	1070
-1	+1	0	-0.54	-70	-1070
+1	0	+1	2.84	320	540
0	+1	+1	2.84	320	-530
-1	0	-1	-3.92	-440	-530
0	-1	-1	-3.92	-440	540
+1	+1	+2	6.22	710	0
-1	-1	-2	-7.30	-810	0

($\alpha \neq 0$) in the detour reflections of the SL-1* and SL+1* satellites, may also reduce their contribution.

4. Conclusions

We have presented here an investigation of the reciprocal space of substrate and superlattice reflections under Bragg surface diffraction. Two interesting results have been obtained. Firstly, the elongations of the substrate rods under BSD due to the attenuation of the X-ray wave field in the surface-detour reflection. The attenuation value, inaccessible by the $\omega:\varphi$ scan technique, could be estimated; it has confirmed that the BSD probe depth is less than $1 \mu\text{m}$ (Hayashi *et al.*, 1997). Secondly, the measurement of BSD in the superlattice has presented a new feature: detour reflection between the superlattice satellites does occur. It gives rise to an effective satellite structure at the same position of the normal satellite structure of the primary reflection. A

further investigation of the effective satellite intensities in several superlattices should be carried out. It will establish if rod scans of superlattices when performed near the multiple diffraction condition have satellite intensities that are significantly affected by the occurrence of effective satellites.

The authors would like to thank FAPESP, FINEP and the Office for International Collaboration (CCInt/USP) for financial support.

References

- Bartels, W. J., Hornstra, J. & Lobeek, D. J. W. (1986). *Acta Cryst.* **A42**, 539–548.
 Bauer, G., Li, J. & Koppensteiner, E. (1995). *J. Cryst. Growth*, **157**, 61–70.
 Chang, S. L. (1984). *Multiple Diffraction of X-rays in Crystals*, in *Springer Ser. Solid-State Sci.*, Vol. 50. Berlin: Springer.
 Fewster, P. (1991). *J. Appl. Cryst.* **24**, 178–193.

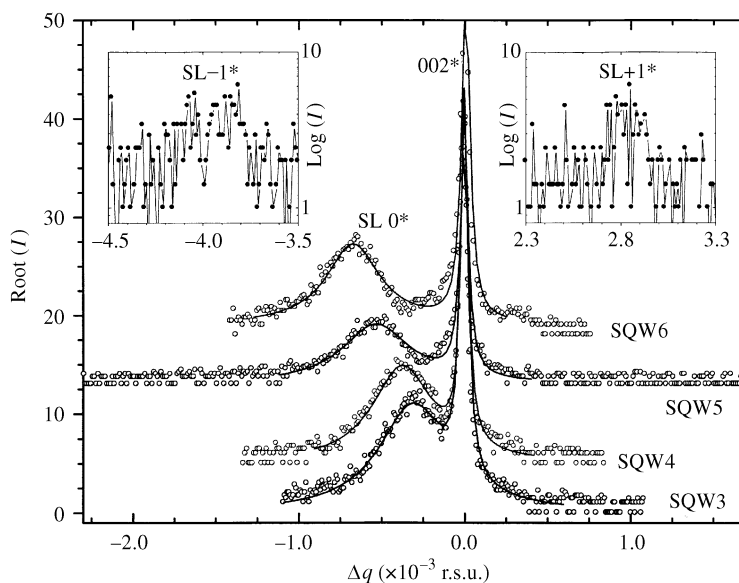


Fig. 6. Rod scans of the 002 reflection under BSD ($\varphi \approx 6^\circ$) for the samples listed in Table 1: experimental (circles) and Lorentzian fit (line). The insets show scans performed without the analyser crystal at the SL+1* and SL-1* positions in the sample SQW5.

- Hayashi, M. A., Morelhão, S. L., Avanci, L. H., Cardoso, L. P., Sasaki, J. M., Kretly, L. C. & Chang, S. L. (1997). *Appl. Phys. Lett.* **71**, 2614–2616.
- Morelhão, S. L. & Cardoso, L. P. (1996). *J. Appl. Cryst.* **29**, 446–456.
- Weckert, E. & Hümmel, K. (1997). *Acta Cryst.* **A53**, 108–153.